

The X-ray properties of high- z FRI candidates in the COSMOS field

E. Tundo^{1*}, P. Tozzi^{1,2} and M. Chiaberge^{3,4}

¹*INAF - Osservatorio Astronomico di Trieste, Via Tiepolo 11, I-34143 Trieste, Italy*

²*INFN - Istituto Nazionale di Fisica Nucleare, Sezione di Trieste, Italy*

³*Space Telescope Science Institute, 3700 San Martin Drive, Baltimore, MD 21218*

⁴*INAF - IRA, Via P. Gobetti 101, Bologna I-40129, Italy*

October 6th, 2011

ABSTRACT

We report the X-ray analysis of a sample of candidate high-redshift ($1 < z < 2$) FRI sources from the sample of Chiaberge et al. (2009), observed in the Chandra COSMOS field (C-COSMOS). Our main goals are to study their nuclear properties by means of unresolved X-ray emission, and to constrain the presence of clusters surrounding the FRI sources from the diffuse X-ray emission by the associated hot plasma. Among 19 FRI candidates, 6 have an X-ray unresolved counterpart in the C-COSMOS catalog. Two additional sources are not present in the C-COSMOS catalog but are clearly detected in the Chandra images. X-ray spectral analysis, when possible, or hardness ratio of the stacked emission from X-ray detected sources, suggest that some of them have significant intrinsic absorption ($N_H \gtrsim 10^{22} \text{ cm}^{-2}$), and high X-ray luminosities with respect to local FRIs. From the stacking analysis of the 11 non-detected sources, however, we find evidence for unresolved soft X-ray emission and no detected hard emission, suggesting an unabsorbed spectrum. Therefore, the X-ray properties vary significantly from source to source among these FRI candidates. From the analysis of the stacked images of all 19 FRI candidates we can rule out the presence of virialized haloes with temperatures larger than 2–3 keV; however, the upper limit on the average extended emission is still consistent with the presence of ~ 1 –2 keV hot gas.

Key words: galaxies: active – galaxies: high-redshift – galaxies: clusters: general – X-rays: galaxies: clusters – radio continuum: galaxies

1 INTRODUCTION

Among the most energetic phenomena in the universe, radio galaxies are expected to play a major role in the study of several topics in astrophysics, such as accretion onto supermassive black holes (SMBH), the associated formation of relativistic jets (e.g. Blandford & Payne 1982; Livio 1999), the feedback processes of an accreting SMBH in the star formation history of a galaxy (e.g. Hopkins et al. 2006) and the role of the Active Galactic Nuclei (AGN) in injecting energy in the intracluster medium (Fabian, Celotti & Erlund 2006). Only recently the possibility of using the connection between Fanaroff-Riley I radio galaxies (FRIs; Fanaroff & Riley 1974) with elliptical massive galaxies in cluster (Owen 1996; Zirbel 1996) has been explored in the frame of the search of clusters in the redshift range $1 < z < 2$ (see Chiaberge et al. 2009, Chiaberge et al. 2010).

Following the AGN unification scheme (Antonucci 1993; Urry & Padovani 1995 and reference therein), radio galaxies are the mis-oriented parent population of jet-dominated blazars, and thus correspond to large viewing angles to the jet/dusty torus axes. Emission from the misaligned sources should be significantly obscured by dust and gas associated with the torus. The centrally-brightened FRI galaxies should be the misaligned versions of BL Lac objects, while most edge-brightened FRIIs are unified with powerful quasars. FRI galaxies typically have a radio power lower than that of FRII sources, with the FRI/FRII break set at $L_{178\text{MHz}} \sim 2 \times 10^{33} \text{ erg s}^{-1} \text{ Hz}^{-1}$ or $L_{1.4\text{GHz}} \sim 4 \times 10^{32} \text{ erg s}^{-1} \text{ Hz}^{-1}$. A more accurate scheme is given by Jackson & Wall (1999), who claim that there are two parent populations, the high radio-power FRII radio galaxies which are the parents of all radio quasars and some BL Lac-type objects, and the moderate-radio-power FRI radio galaxies which are the parents of the majority of BL Lac-type objects. The transition between FRIs and FRIIs is anyway rather smooth and both radio morphologies are present in

* mail: tundo@oats.inaf.it (ET); tozzi@oats.inaf.it (PT), marcoc@stsci.edu (MC)

the population of sources around the break. The FRI/FRII break (at low redshift) also depends on the luminosity of the host galaxy, as shown by Owen & Ledlow (1994) and Ledlow & Owen (1996). However, it is still unclear whether or not that might simply be a result of selection effects (Scarpa & Urry 2001).

As a further complication, objects of intermediate radio structure do exist (e.g. Capetti, Fanti & Parma 1995), and a class of hybrid double sources, with a FRI jet on one side and a FRII lobe on the other, was also unveiled by Gopal-Krishna & Wiita (2000). This supports explanations for the FR dichotomy based upon different jet interaction with the Inter Galactic Medium of the same nuclear engine (Kaiser & Alexander 1997, Gawroński et al. 2006, Evans et al. 2008). On the other hand, in some models the different radio power is expected to be associated to different accretion modes, with FRIIs being powered by a standard accretion disc and FRIs by an advection dominated accretion flow (see Reynolds et al. 1996; Ghisellini & Celotti 2001).

Apart from their intrinsic properties, FRIs and FRIIs differ also in their typical environment. The FRI and FRII host galaxies are mostly elliptical massive galaxies in the local universe (e.g. Zirbel 1996; Donzelli et al. 2007), and thus are associated with the most massive black holes in the local universe through the $M_{\bullet}-\sigma_*$ relation (Ferrarese & Merrit 2000, Gebhardt et al. 2000, Tremaine et al. 2002). However, FRIs are usually located at the centre of massive clusters (see e.g. Owen 1996, for a review). For example, 94% of the radio sources in the central regions of Abell clusters are FRIs (Ledlow & Owen 1996). On the contrary, FRIIs at low redshift are generally found in regions of lower density, with an increasing fraction of FRII residing in rich groups or clusters only at redshift higher than ~ 0.5 (Prestage & Peacock 1988; Zirbel 1996; Hill & Lilly 1991; Best 2007). In addition FRII host galaxies show an optical morphology often associated with violent galaxy encounters, with a low percentage of smooth ellipticals (Zirbel 1996).

In this framework, FRIs can be successfully used as a tool in the search for high redshift clusters. However, so far this aspect has not been exploited properly (see Chiaberge et al. 2009). The optical search for clusters of galaxies at $z > 1$ has proven to be particularly difficult, mainly because of the reduced contrast between cluster members and field galaxies. In order to tackle this difficulties, high- z clusters have been recently searched using the so-called red sequence technique (Gladders & Yee 2000). With a similar approach extended to longer wavelengths, Eisenhardt (2008) presented a sample of clusters of galaxies from the Spitzer Infrared Array Camera Shallow Survey. Among their 335 cluster candidates, 18 have confirmed spectroscopic redshift $z \sim 1.1-1.4$, and a few have photometric redshift (obtained using photometry in 4 bands, B_W , R , I , and $3.6\mu\text{m}$) in the range $z_{\text{phot}} \sim 1.5-2$. A similar effort is being pursued by the Spitzer Adaptation of the Red-Sequence Cluster Survey (SpARCS¹) project. Their cluster detection algorithm lead to about two hundred high z cluster candidates, and the follow-up and analysis phase, which will last for several years, had spectroscopically confirmed about a dozen clusters at $z > 1$ so far (see Wilson et al. 2009; Muzzin et al. 2009; Demarco et al.

2010). Turning to the X-ray window explored by the Chandra, XMM and Swift satellites, several new detections are found based on the compilation of serendipitous medium and deep-exposure extragalactic pointings not associated to previously known X-ray clusters. Among them, the XMM Deep Cluster Survey (XDCP², Fassbender et al. in prep. that has so far spectroscopically confirmed 18 clusters at $z > 0.8$), the ChaMP Serendipitous Galaxy Cluster Survey (Barkhouse et al. 2006), and the Swift-XRT Cluster Survey (SXCS, Tundo et al., Moretti et al. in prep.). In addition, there are also ongoing dedicated surveys like the XMM-BCS cluster survey (Suhada et al. 2011, in prep.), and the XMM Large Scale Structure Survey (XMM-LSS; Pierre, Valtchanov & Refregier 2002). So far, the highest confirmed redshift for an X-ray detected cluster is $z \sim 1.62$ (Tanaka et al. 2010), with a few extreme candidates at $z \sim 2$ (see, e.g., Andreon & Huertas-Company 2011). To summarize, the present-day limit for the detection of well characterized, virialized cluster of galaxies, is $z \gtrsim 1.5$.

Given the properties of the environment of local FRIs and their association with massive ellipticals in clusters at $z \sim 0$, FRIs may help in the search of high redshift clusters at $z \gtrsim 1.5$. In Chiaberge et al. (2009; 2010) the selected sample of FRIs in the COSMOS field (Scoville et al. 2007) is used to search for cluster candidates in this relatively unexplored redshift range. With this study we want to exploit the Chandra X-ray data in the COSMOS field to investigate the X-ray properties of the FRI sample of Chiaberge et al. (2009). Thanks to the deep C-COSMOS X-ray images, this work carries out a study to investigate both the intrinsic properties of FRIs at high redshift and the presence of Intra Cluster Medium emission associated to possible clusters hosting the FRIs.

The Paper is organized as follows. In §2 we present the sample; in §3 we study the photometric X-ray properties of the FRI candidates and the spectral analysis of the 8 sources with unresolved X-ray counterparts. In §4 we explore the possibility of detecting extended emission with a stacking analysis. Finally in §5 we summarize our results. We use a standard flat Λ CDM cosmological model with the best-fit parameters from the seven years WMAP data $\Omega_m = 0.272$, $\Omega_\Lambda = 0.728$, and $H_0 = 70.4 \text{ km s}^{-1} \text{ Mpc}^{-1}$ (Komatsu et al. 2011).

2 THE SAMPLE

Chiaberge et al. (2009) selected a sample of 37 high redshift ($1 < z < 2$) FRI candidates in the COSMOS field. They proceeded in four steps, under few basic assumptions. The two main assumptions are: the FRI/FRII break in radio power per unit frequency does not change with redshift; the photometric properties of the hosts of FRIs at $1 < z < 2$ are similar to those of FRIIs within the same redshift bin, as in the case of local radio galaxies (e.g. Donzelli et al. 2007).

They selected FIRST radio sources (see Becker, White & Helfand 1995) in the COSMOS field according to their 1.4 GHz flux. Sources are considered FRI candidates when the 1.4 GHz flux falls within the range of fluxes expected

¹ <http://www.faculty.ucr.edu/~gillianw/SpARCS/>

² http://www.xray.mpe.mpg.de/theorie/cluster/XDCP/xdcp_index.html

Table 1. FRI sources in the C-COSMOS field: (1) FRI candidates Id (Chiaberge et al. 2009); (2) C-COSMOS X-ray catalog Id (if present) (3),(4) RA DEC coordinates of the FRI candidates; (5) photometric redshift (Ilbert et al. 2009).

FRI	C-COSMOS ^a	Ra	Dec	z_{phot} ^b
01		150.20744	2.28187	$0.883^{+0.004}_{-0.004}$ † ‡
03	451	150.00253	2.25863	$2.09^{+0.01}_{-0.01}$ *
04		149.99153	2.30277	$1.45^{+0.04}_{-0.02}$
05	1091	150.10612	2.01447	$1.88^{+0.03}_{-0.05}$ *
07		150.26883	2.03435	$0.94^{+0.02}_{-0.02}$
11		150.07816	1.89855	$1.31^{+0.13}_{-0.08}$
13	1242	149.97784	2.50420	$1.171^{+0.04}_{-0.06}$ *
16		150.53772	2.26735	$0.969^{+0.001}_{-0.001}$ †
18	427	149.69325	2.26746	$0.904^{+0.04}_{-0.02}$ *
20		149.83209	2.56954	$0.99^{+0.06}_{-0.02}$
22		149.89508	2.62921	$1.79^{+0.03}_{-0.02}$
26		149.62114	2.09198	$1.19^{+0.01}_{-0.01}$
28		149.60064	2.09186	$1.23^{+0.11}_{-0.06}$
29		149.64587	1.95297	$1.59^{+0.18}_{-0.15}$
30		149.61542	1.99105	$0.90^{+0.02}_{-0.01}$
31		149.61916	1.91636	$0.913^{+0.001}_{-0.001}$ † ‡
32		149.66830	1.83797	$0.58^{+0.01}_{-0.22}$
52	701	149.90590	2.39647	$0.74^{+0.01}_{-0.01}$ *
66	669	149.95946	1.80149	$0.68^{+0.01}_{-0.01}$ *

^a FRI sources 1 and 4, while not present in the C-COSMOS catalog, have a robust X-ray counterpart.

^b †: spectroscopic redshift from the zCOSMOS catalog (Lilly et al. 2007); ‡: spectroscopic redshift from Magellan-COSMOS (Trump et al. 2007); * photometric redshift from Salvato et al. (2011).

for FRIs at $1 < z < 2$. This criterion is $1 < F_{1.4} < 13$ mJy. From the analysis of the VLA-COSMOS (Schinnerer et al. 2007) images, sources with FRII radio morphology were excluded. Bright ($m_I > 22$) galaxies were rejected as likely low- z galaxies with intrinsically faint radio emission (e.g. nearby starbursts), and U-band dropouts were rejected as likely to be at $z > 2.5$. This lead to the final sample of 37 FRI candidates.

In this work we search for the X-ray counterparts of the FRI candidates included within the Chandra COSMOS Survey (C-COSMOS, Elvis et al. 2009). The C-COSMOS is a large, 1.8 Ms, Chandra program that has imaged the central 1 deg^2 of the COSMOS field (centred at $10^h00^m28.6^s$, $+02^\circ12'21.0''$, and overlapping with a region of 2 deg^2 imaged with XMM-Newton, see Cappelluti et al. 2009). This results in an average exposure of ~ 160 ksec in the inner 0.5 deg^2 region, and an outer 0.5 deg^2 area with an effective exposure of ~ 80 ksec. The limiting fluxes for point source detection are $1.9 \times 10^{-16} \text{ erg cm}^{-2} \text{ s}^{-1}$ in the soft (0.5-2 keV) and $7.3 \times 10^{-16} \text{ erg cm}^{-2} \text{ s}^{-1}$ in the hard (2-10 keV) band.

XMM-COSMOS (Hasinger et al. 2007) would indeed offer a bigger effective area than Chandra. However, identification of potential extended sources, in particular at medium and high redshift, is more difficult than with Chandra, due to the size of the XMM Point Spread Function (PSF, whose Half Energy Width is $15''$ at the aimpoint) and its degradation as a function of the off-axis angle. Moreover, the sharp PSF of Chandra makes easier to identify faint point

sources which otherwise may be confused with the possible diffuse emission. Therefore, we decide to limit our study to the Chandra data only.

Only 19 out of the 37 FRI candidates are included in the C-COSMOS field. Starting from the C-COSMOS source list (Elvis et al. 2009), we searched for all the possible X-ray counterparts within a matching radius of 2 arcsec. The number of expected false matches is negligible thanks to the low number density of the X-ray and radio sources at the limiting fluxes. Table 1 lists the FRI candidates studied in this work, with their X-ray counterparts when present. We find the X-ray counterparts in the C-COSMOS point source catalog for 6 radio sources. In addition, the two radio sources FRI 1 and 4, have highly significant X-ray counterparts which are not listed in the C-COSMOS catalog. The photometric redshifts are given by Ilbert et al. (2009) for all the sources without a C-COSMOS counterpart. For three sources we also have a spectroscopic redshift from the zCOSMOS catalog (Lilly et al. 2007) or the Inamori Magellan Area Camera and Spectrograph instrument on the Magellan telescope (Trump et al. 2007). For sources with a C-COSMOS counterpart we use the photometric redshift of Salvato et al. (2011).

3 X-RAY ANALYSIS

The X-ray data are processed in a standard way using the *ciao* 4.3 software and the calibration database CALDBv4.4.5. We obtained the merged image of the entire C-COSMOS field, and performed aperture photometry on the radio position for our sample of FRI candidates. The results are given in Table 2 for the soft (0.5-2 keV) and hard (2-10 keV) X-ray bands. The net counts and the signal-to-noise ratio (S/N) are computed within an extraction radius of 5 arcsec unless this radius overlap with a nearby bright source. We use a smaller aperture only for FRI 4 whose extraction radius was set to 3.5 arcsec. The quoted uncertainties represent the 84.13% upper and lower confidence level assuming a Poisson distribution, that correspond to 1 σ level in the Gaussian statistics (see Gehrels 1986). For sources without an X-ray counterpart we report the corresponding 3 σ upper limit (in these cases S/N and hardness ratio are not defined). Count rates and energy fluxes in the soft and hard bands are corrected for vignetting using the composite monochromatic exposure maps computed at 1.5 and 4.5 keV, respectively. The hardness ratio is computed as $HR = (H - S)/(H + S)$, where H and S are the aperture photometry in the hard and soft band, respectively. Approximate energy fluxes are computed directly from the measured count rate as in Rosati et al. (2002), using conversion factors corresponding to a slope of $\Gamma_{av} = 1.4$, that represents the average spectral shape for X-ray sources in the $10^{-16} - 10^{-15} \text{ erg s}^{-1} \text{ cm}^{-2}$ flux range (see Tozzi et al. 2001). Note that this value is meant to include the average effect of the intrinsic absorption among the AGN population, and it is different from the adopted value for the slope of the intrinsic emission $\Gamma = 1.8$. Luminosities are calculated adopting the photometric redshift of Ilbert et al. (2009) and Salvato et al. (2011), and the spectroscopic redshift from the zCOSMOS e Magellan-COSMOS catalogs when available.

Among the 19 FRI candidates observed in the C-

Table 2. X-ray aperture photometry for FRI candidates: (1) FRI candidate Id (Chiaberge et al. 2009); (2),(3) soft and hard net counts with 1σ Poissonian error bars; (4),(5) soft and hard Signal to Noise Ratio; (6) Hardness Ratio; (7),(8) observed soft and hard flux corresponding to an average spectral slope of $\Gamma_{av} = 1.4$; (9),(10) observed soft and hard luminosities. X-ray fluxes and luminosities for FRI sources with no X-ray counterparts correspond to a 3σ Poissonian upper limit. Uncertainties on luminosities include also the error in the z_{phot} .

FRI Id	Cts _S	Cts _H	S/N _S	S/N _H	HR	S _{0.5–2}	S _{2–10}	L _{0.5–2}	L _{2–10}
						10^{-16} erg cm ⁻² s ⁻¹		10^{42} erg s ⁻¹	
07	< 9.9	< 12.4	–	–	–	<3.1	<18.3	< 1.8± 0.1	< 10.7± 0.6
11	< 8.2	< 16.4	–	–	–	<2.8	<25.6	< 3.9± 0.9	< 36.4± 7.5
16	< 6.9	< 8.2	–	–	–	<5.4	<29.8	< 3.5± 0.02	< 18.9± 0.1
20	<11.9	< 9.1	–	–	–	<7.7	<27.5	< 5.3± 0.2	< 18.8± 0.7
22	< 8.2	< 9.1	–	–	–	<8.5	<34.4	< 28.7± 1.5	< 148.7± 8.0
26	< 7.0	< 8.3	–	–	–	<4.6	<25.1	< 5.1± 0.1	< 28.1± 0.6
28	< 9.2	< 11.3	–	–	–	<6.3	<35.5	< 57.2± 4.5	< 325.3± 23.5
29	< 4.0	< 11.9	–	–	–	<1.9	<26.4	< 4.5± 1.0	< 63.2± 15.5
30	< 8.2	< 8.1	–	–	–	<5.3	<24.6	< 2.8± 0.1	< 12.8± 0.5
31	< 8.2	< 9.2	–	–	–	<8.9	<46.3	< 4.8± 0.3	< 24.9± 0.5
32	< 7.0	< 11.3	–	–	–	<5.1	<38.2	< 0.8± 0.3	< 6.3± 3.5
01	5.4 ^{+4.4} _{-3.6}	8.9 ^{+5.6} _{-4.6}	1.55	1.89	0.25 ^{+0.5} _{-0.7}	1.6±1.0	12.8± 6.6	0.8± 0.5	6.3± 3.4
03	35.73 ^{+7.3} _{-6.3}	85.06 ^{+10.8} _{-9.8}	5.65	8.73	0.41 ^{+0.2} _{-0.2}	12.4±2.1	137.8±15.6	52.8±11.2	583.2±102.9
04	9.0 ^{+4.3} _{-3.3}	3.7 ^{+3.8} _{-2.8}	2.72	1.39	-0.41 ^{+0.8} _{-0.5}	3.1±1.0	6.6± 4.0	5.8± 2.0	12.4± 8.0
05	15.27 ^{+5.4} _{-6.1}	16.22 ^{+6.0} _{-5.0}	3.50	3.31	0.03 ^{+0.4} _{-0.5}	5.2±1.4	27.1± 7.4	19.9± 5.7	103.2± 30.0
13	12.43 ^{+5.0} _{-4.0}	13.94 ^{+5.9} _{-4.9}	3.11	2.85	0.06 ^{+0.5} _{-0.5}	3.8±1.2	19.3± 6.9	4.0± 1.3	20.4± 7.5
18	10.63 ^{+4.4} _{-3.4}	0.6 ^{+2.9} _{-0.6}	3.07	0.29	-0.90 ^{+0.7} _{-0.1}	7.8±2.5	0.7± 7.3	4.0± 1.3	0.4± 3.5
52	29.80 ^{+6.7} _{-5.7}	14.65 ^{+5.7} _{-4.7}	5.19	3.12	-0.34 ^{+0.4} _{-0.3}	10.6±2.0	23.7± 7.9	3.3± 0.6	7.4± 2.3
66	1.13 ^{+2.7} _{-0.9}	9.14 ^{+4.6} _{-3.6}	0.65	2.54	0.78 ^{+0.2} _{-0.9}	0.7±1.1	27.3±10.7	0.2± 0.3	6.8± 2.7

COSMOS field, 13 have no X-ray counterparts in the COSMOS X-ray point source catalog. Among them, FRI 1 and 4 are not included in the C-COSMOS catalog, probably due to their proximity with bright sources; despite this, they have robust X-ray counterparts with about 15 net counts from our aperture photometry. Uncertainties in the photometric redshifts have been propagated to the luminosities using a Monte Carlo simulation. On average, we have a relative error on the X-ray luminosity of about 30%, mainly due to poor S/N.

We investigate the X-ray properties of the 11 FRI candidates with no clearly detected X-ray emission. We produced soft and hard stacked X-ray images, shown in Figure 1, adding the position of the 11 radio sources after masking all the C-COSMOS X-ray sources. The stacked images show a signal in the soft band, while none is visible in the hard band. We tested the robustness of the procedure by stacking random positions in the masked C-COSMOS image. We measure positive emission at a 2σ level in the soft band, with 9 ± 4 net counts, and formally zero flux in the 2-7 keV band, (6 ± 5 net counts), in agreement with the single source aperture photometry. This very weak signal can not be used to infer information on the spectral shape, nevertheless, it is compatible with no absorption at all. Since there are 8 FRI candidates with detected X-ray emission, one would expect to measure a larger X-ray signal in the stacked images if the average X-ray properties were the same for all the FRI sample. This difference can not be explained by lower effective exposure times for the non-detections. In fact, after normalizing their count rate to the average exposure time, the stacked signal of the 11 FRI without X-ray counterpart is only 13 and 9 net counts in the soft and hard band, respectively. This shows that the X-ray properties vary sig-

nificantly from source to source among the FRI candidates, with more than half of them showing no X-ray emission at all.

We can push further the investigation of the X-ray properties of the FRI candidates with X-ray detection, with a detailed spectral analysis using *Xspec* v12.6.0. Since each source is observed in several exposures, each spectrum is obtained by adding the spectra extracted from each observation using the standard FTOOLS (Blackburn 1995) routines. Spectra are extracted from a circular region with a fixed radius of 5 arcsec. Local background regions were extracted from annuli around the X-ray sources with an inner and external radii of 7 and 12 arcsec, respectively, after masking nearby X-ray sources to avoid contamination. The effective area and response files are created for each observation and then combined using the FTOOLS routines ADDARF and ADDRMF.

The adopted spectral model is an absorbed power law, with a fixed Galactic absorption. The value of the Galactic absorption is $N_H = 1.7 \times 10^{20}$ cm⁻², obtained as the average value in the C-COSMOS region measured in the Leiden/Argentine/Bonn survey (Kalberla et al. 2005). Given the low S/N of our spectra, the intrinsic power law index is fixed to $\Gamma = 1.8$, which is the average value found in AGN in a similar flux range (see, e.g., Tozzi et al. 2006). FRI 1, 4, 18 and 66 are detected with a number of net counts too low (about 10-15 in the 0.5-7 keV band) to have a meaningful spectral analysis. We note also that these sources have the lowest exposure time among the sources with an X-ray counterpart. Best fit parameters are found by minimizing the Cash's *C*-statistic (Cash, 1979; Nousek & Shue, 1989) which is appropriate for low S/N. We also report a goodness parameter to evaluate the quality of the fit performed

Table 3. Spectral analysis for the FRI candidates with an X-ray detected emission with $\gtrsim 30$ Net Counts: (1) FRI Id; (2) C-COSMOS Id; (3) total net counts; (4) intrinsic absorption; (5),(6) soft and hard fluxes; (7)(8) soft and hard intrinsic luminosity; (9) Goodness parameter

FRI	C-COSMOS	Net Cts	N_H 10^{22} cm^{-2}	$S_{0.5-2}$ $10^{-16} \text{ erg cm}^{-2} \text{ s}^{-1}$	S_{2-10} $10^{-16} \text{ erg cm}^{-2} \text{ s}^{-1}$	$L_{0.5-2}$ $10^{42} \text{ erg s}^{-1}$	L_{2-10} $10^{42} \text{ erg s}^{-1}$	goodness
03	451	124^{+25}_{-23}	35^{+5}_{-5}	11.0 ± 2.0	138 ± 14	196 ± 35	445 ± 49	5%
05	1091	34^{+16}_{-14}	7^{+6}_{-4}	4.7 ± 1.3	18 ± 5	20 ± 6	42 ± 12	47%
13	1242	26^{+16}_{-13}	8^{+3}_{-3}	3.2 ± 1.0	25 ± 8	10 ± 3	17 ± 6	48%
52	701	38^{+17}_{-14}	$1.7^{+0.6}_{-1}$	7.3 ± 1.3	24 ± 7	4.3 ± 1.0	6 ± 2	3%

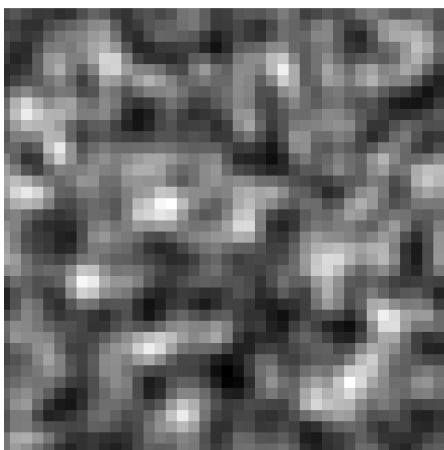
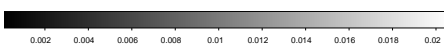
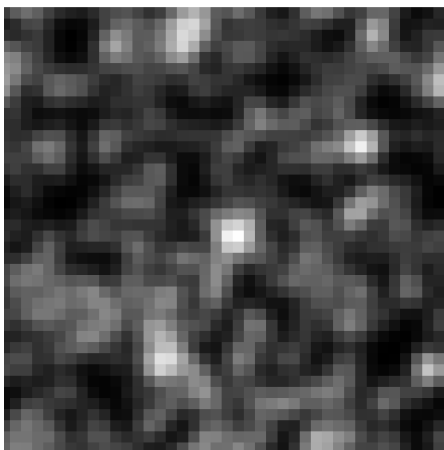


Figure 1. Upper panel: smoothed stacked image in the soft (0.5–2 keV) band of the 11 FRI candidates without X-ray detection (see text for details). Lower panel: the same as in the upper panel for the 2–7 keV band. The size of the images is 40×40 arcsec.

within **Xspec** by means of Monte Carlo simulations³. When the best-fit is acceptable, the *goodness* parameter is around 50%. In Table 3 we report the results of our spectral analysis. In Figure 2 we show the spectral fits for FRI candidates 3, 5, 13 and 52.

Fluxes derived from fits to the spectral template are in agreement with the fluxes obtained directly from the count rate with an average conversion factor (see Table 2). All the examined sources are consistent with being absorbed at the level of a few $\times 10^{22} \text{ cm}^{-2}$, with source FRI 3 having $N_H = 3.5 \pm 0.5 \times 10^{23} \text{ cm}^{-2}$.

We further explore the spectrum of FRI 3, which is the source with the largest number of counts. We relax the constraints on the intrinsic power law Γ , finding $\Gamma = 1.6 \pm 0.8$ and $N_H = 2.6 \pm 0.4 \times 10^{23} \text{ cm}^{-2}$, with a slight improvement in the quality of the fit. The best fit obtained with a reflection-dominated spectral model (PEXRAV) shows only a modest increase in the quality of the fit, but with an unrealistic value for the intrinsic slope $\Gamma \sim 0$.

Given the poor S/N of sources FRI 5, 13 and 52, the errors on the measured N_H are quite large, and all the best-fit values are consistent with no absorption within 2σ . In order to get a lower limit on the average absorption, we stack the signal of all the radio sources with X-ray counterpart with the exception of FRI 3. We obtain a total of 88 ± 10 and 73 ± 11 net counts in the soft and hard bands, respectively. This correspond to $HR = -0.09 \pm 0.09$. Since the average redshift of this 7 sources is $\langle z \rangle = 1.09$, we can estimate the average absorption by comparing the HR values seen by Chandra as a function of intrinsic N_H for that redshift. We find an average $N_H = 3.1 \pm 1.2 \times 10^{22} \text{ cm}^{-2}$. This shows that the average intrinsic absorption the in the X-ray detected FRI sources is $N_H \geq 10^{22} \text{ cm}^{-2}$ at 2σ confidence level.

Therefore, we find that at least some of the FRI candidates, namely those with X-ray counterparts in the C-COSMOS data, show sign of significant intrinsic absorption, at a level typically higher than those found in local FRIs (Donato et al. 2004, Balmaverde et al. 2008). Donato et al. (2004) found 8 FRI sources out of 25 with excess absorption over the Galactic value with rest-frame column densities $N_H \sim 10^{20} - 10^{21} \text{ cm}^{-2}$, and no sources with $N_H \sim 10^{22} \text{ cm}^{-2}$. The power law photon index of their sample spans in the range of values $\Gamma \sim 1.1 - 2.6$, with average value $\Gamma = 1.9$ and standard deviation $\sigma = 0.4$. Balmaverde et al. (2008) detected nuclear X-ray absorption at a level of

³ <http://heasarc.gsfc.nasa.gov/docs/xanadu/xspec/manual/XSgoodness.html>

Table 4. Radio Power for the FRI candidates: (1) FRI Id; (2) C-COSMOS Id (if present); (3) observed FIRST flux (mJy) at 1.4GHz, from Table 1 in Chiaberge et al. (2009); (4) rest frame luminosity at 1.4GHz.

FRI	C-COSMOS	$S_{1.4GHz}$ mJy	$L_{1.4GHz}$ $10^{32} \text{ erg s}^{-1} \text{ Hz}^{-1}$
07		5.99	6.706
11		1.3	2.543
16		1.14	0.4483
20		1.13	0.985
22		1.51	0.853
26		5.7	2.417
28		4.39	1.627
29		1.33	0.6055
30		2.74	5.063
31		1.88	1.329
32		1.77	7.725
<hr/>			
01		1.79	0.6074
03	451	2.12	2.952
04		4.21	9.528
05	1091	1.26	0.4523
13	1242	3.71	1.364
18	427	1.31	0.1628
52	701	1.54	0.3443
66	669	1.11	0.2043

$N_H \sim (0.2-6) \times 10^{22} \text{ cm}^{-2}$ in 4 out of 18 FRI sources. They observe that X-ray absorbed sources in their sample of low-luminosity 3C/FRI galaxies are associated with the presence of highly inclined dusty discs seen in the HST images, and suggest the existence of a flattened X-ray absorber, but of much lower optical depth than in classical obscuring tori. In their sample, they found a range of $\Gamma \sim 0.8-2.4$, again with average value $\Gamma=1.9$ and standard deviation $\sigma=0.5$.

X-ray unabsorbed luminosities span a range of values larger than those observed in low redshift FRIIs. Donato et al. (2004) report just 7 out of 25 sources with luminosities $L_X \leq 10^{42} \text{ erg sec}^{-1}$ in the 0.3–8 keV band, and only 2 with luminosities $L_X \sim 10^{43} \text{ erg sec}^{-1}$. Balmaverde et al. (2008) report only one FRI source with $L_X \gtrsim 10^{43} \text{ erg sec}^{-1}$ in the 0.5–5 keV band.

To summarize, the FRI candidates presented in Chiaberge et al. (2009) show X-ray characteristics that vary significantly from source to source. In this sample 11 sources out of 19 have no X-ray counterpart, but they are detected at a 2σ confidence level in their stacked soft-band image, while they are still not detected in their stacked hard band image. Therefore, they do not show any hint of being absorbed AGN. On the other hand, radio sources with X-ray counterpart show significant intrinsic absorption from single-source spectral analysis, and the hardness ratio of the stacked image suggests an average $N_H \simeq 10^{22} \text{ cm}^{-2}$. Among them, FRI sources 3, 5 and 13 show higher intrinsic luminosities, while FRI 1, 4, 18, 55 and 66 have luminosities comparable to that of low- z FRIIs. Both luminosities and intrinsic absorption reach values that are unfrequently observed in low- z sources.

However, we note that we are studying a sample that might include a few objects with radio power more typical of the FRII population. The 1.4GHz radio luminosity of the FRI candidates in our sample is shown in Ta-

ble 4. We assumed a power law energy index $\alpha \sim 0.8$. We note that among the sources with X-ray counterpart, two are within a factor of 2 of the FRI/FRII break luminosity $L_{break}(1.4GHz) \sim 4 \times 10^{32} \text{ erg s}^{-1} \text{ Hz}^{-1}$, while the remaining 4 have radio luminosities ten times lower than L_{break} . The highest absorption and luminosity is measured for the radio source with $L_{1.4GHz} \sim L_{break}$. Despite our sample may include some FRIIs, we cannot exclude a possible evolution of the X-ray properties of FRI sources, suggesting that the accretion in high redshift FRIIs may be different with respect to low redshift ones. In particular, the presence of a dusty torus in high redshift FRIIs could explain the fraction of highly absorbed sources. In low- z FRIIs, the presence of a dusty torus is usually rejected on the basis of the low intrinsic absorption typically measured at X-ray wavelengths (Donato et al. 2004), and of the high optical-core detection rate (Chiaberge, Capetti & Celotti 1999). However, several works (Hardcastle et al. 2002; Evans et al. 2006) point out that a jet dominated X-ray emission occurring on scales larger than a torus (therefore mimicking low absorption) cannot be excluded, and this leaves room to the presence of the torus. Another possible explanation is that we may be observing a sort of intermediate population, with characteristics that are in-between FRIIs and FRIIs, with a radio morphology typical of low redshift FRIIs and with X-ray properties more typical of FRIIs. Such sort of intermediate objects are already known (Capetti, Fanti & Parma 1995).

4 SEARCH FOR X-RAY EXTENDED EMISSION

Under the assumption that the environment of FRIIs does not change with redshift, high- z FRIIs can be used as signposts for high- z clusters. This aspect can be particularly relevant for redshift $z \sim 1.5$ and higher, an epoch still out of reach of current cluster surveys, both in the IR and in the X-ray. The typical flux level of the ICM from a hot ($kT > 5 \text{ keV}$) clusters at $z \sim 1.5$ is $F_{0.5-2keV} \sim 1-2 \times 10^{-14} \text{ erg s}^{-1} \text{ cm}^{-2}$; the stacking technique virtually multiply the effective exposure time by the number of FRI sources, so that the stacked ICM emission, if present, would reach fluxes as high as $10^{-13} \text{ erg s}^{-1} \text{ cm}^{-2}$.

We create stacked images using all the 19 FRI candidates; the stacked images are shown in Figure 3. A visual inspection shows no clear signs of extended emission in the soft band. The same is found in the hard band, where the ICM emission is expected to be much weaker in any case. To provide a quantitative measure, we compute the count rate in the soft band in annuli with inner and outer radii separated by 1 arcsecond. Then we compare these values to those found in images obtained stacking random positions from the masked image. Figure 4 show the soft-band count rate in each annulus of the stacked image of the FRI sources versus the mean value measured in the control-image. We find evidence for emission only within 4 arcsec, while the emission at larger radii is consistent with noise. The stacked image is consistent with unresolved sources imaged at different off axis angle, due to an average Point Spread Function with FWHM of $\sim 2.5 \text{ arcsec}$.

However, the failed detection of extended emission does not rule out the presence of a virialized halo around the FRI

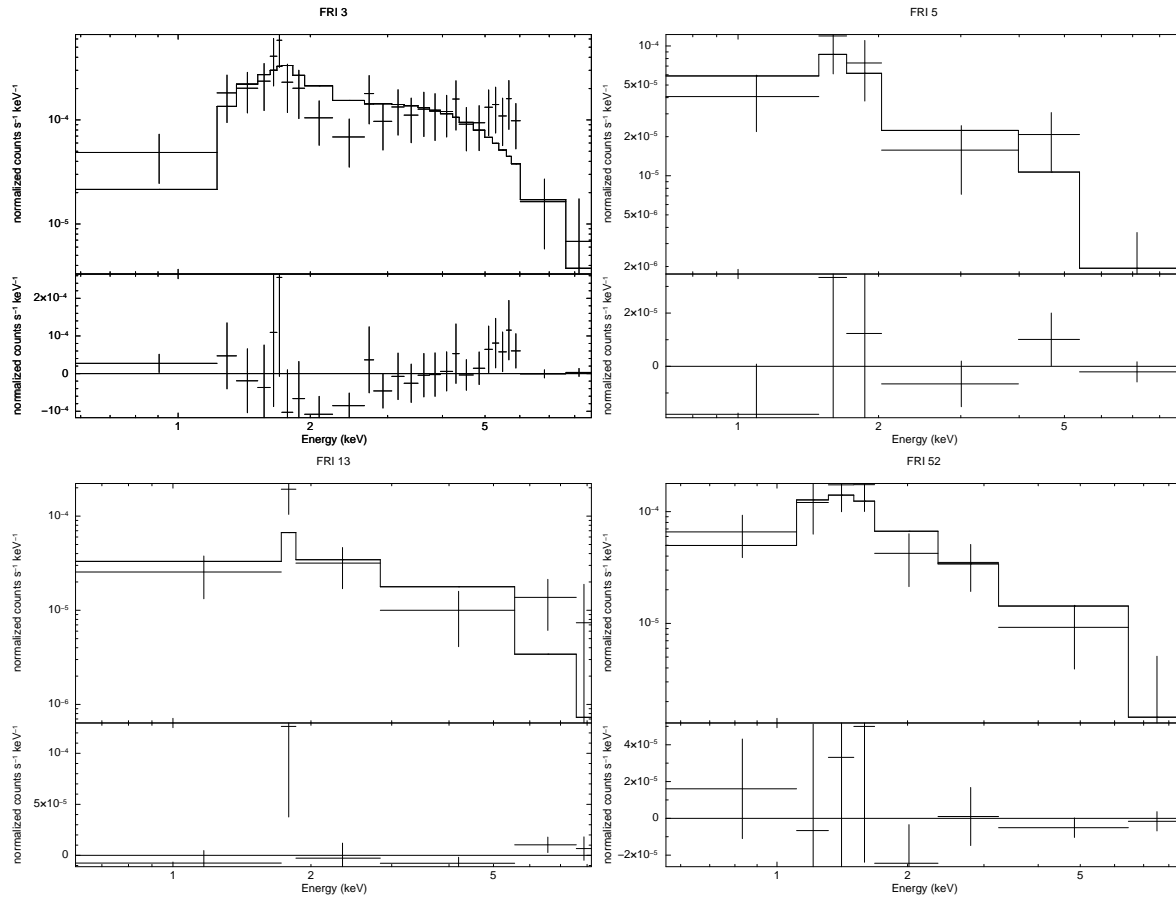


Figure 2. Spectral data and best-fit models with residuals for FRI sources 3 (upper left), 5 (upper right), 13 (bottom left), 52 (bottom right).

sources. To put a robust upper limit to the extended emission that can be allocated around the FRI candidates, we proceed as follows. We associate to each FRI source the typical X-ray emission of a group or cluster at a given temperature. In order to model this ICM emission, we use the Chandra images of real clusters and groups of galaxies cloned to the redshift of the FRI sources. This technique has been already used to investigate the evolution of cool cores at high redshift (see Santos et al. 2008). We used 3 different clusters as template: A907 with a temperature of 5 keV and a luminosity of 4.7×10^{44} erg s $^{-1}$ (typical of rich clusters); A2717 with a temperature of 2.4 keV and a luminosity of 0.78×10^{44} erg s $^{-1}$ (typical of small clusters); and RXJ1320 with a temperature of ~ 1 keV and a luminosity of 0.26×10^{44} erg s $^{-1}$ (appropriate for galaxy groups). The cluster image is cloned to the corresponding FRI redshift and rotated randomly. The nuclear emission is not added to the mock image. The measured count rate for the stacked clones in the annuli, compared to the result from FRI stacked image, is shown in Figure 5. The top, middle and bottom panels show the images obtained using clusters A907, A2717 and RXJ1320, respectively.

In the hypothesis that FRIs are inside clusters with typical temperature around 5 keV (top panels), the stacked image of 19 of those would have shown significant emission at large radii. Therefore, we can rule out such an hypothesis.

The mock image obtained with clones of low temperature clusters ($kT \sim 2.5$ keV) shows some excess with respect to the FRI stacked image at radii larger than 4 arcsec. Still, the two profiles do agree within the uncertainties, also considering that in the local universe about 70% of the FRI galaxies are found in clusters (Zirbel 1996). As a consequence, these results do not rule out the possibility of some of the FRIs being at the centre of medium cluster of typical temperature $kT \sim 2 - 3$ keV. Finally, the mock image corresponding to groups of about 1 keV (see bottom panels of Figure 5) is consistent with the real stacked image, since only the innermost bin would bring the signal of the faint ICM associated to high-redshift groups. In this last case the emission observed in the FRI stacked image in the first bins must be in part associated to the ICM emission of the putative virialized group surrounding the FRI source. The fraction of ICM emission is predicted to be about 20 per cent. This is still compatible with the spectral analysis of FRI sources, despite the detection of intrinsic absorption shows that the majority of the X-ray emission in the inner 5 arcsec must be due to nuclear activity.

To summarize, we obtained constraints to the presence of virialized haloes with ICM emission around FRIs in this sample. There is no room for virialized haloes with $kT \simeq 5$ keV, while group-sized, low temperature ($kT \leq 2$ keV) ICM emission appears to be consistent with the X-ray observa-

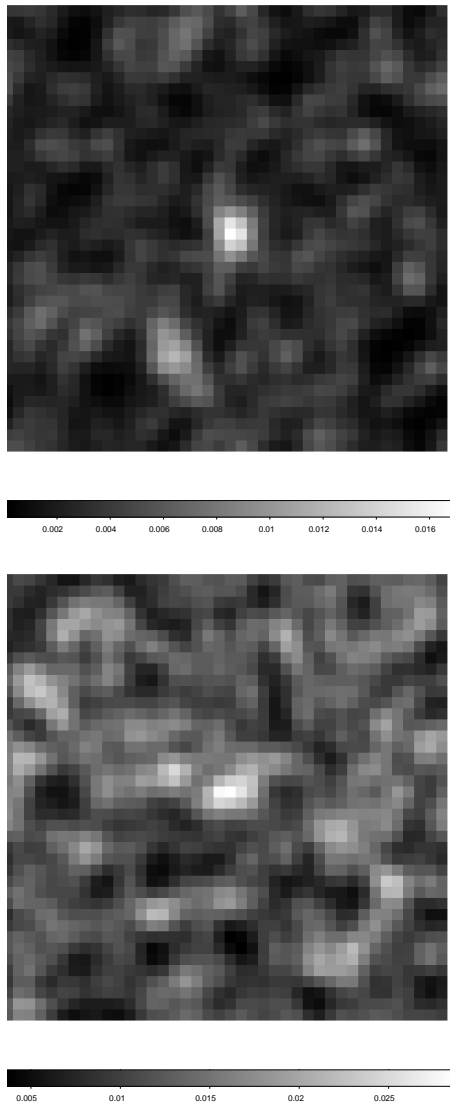


Figure 3. Smoothed stacked images in the soft (upper panel) and hard band (bottom panel) of all the 19 FRI candidates. The size of the images is 40×40 arcsec.

tions of our FRI sample. Much deeper X-ray data are needed to search for this faint emission around FRIs. A similar project in the CDFS 4Ms field (Xue et al. 2011) is currently underway.

5 CONCLUSIONS

We analysed the X-ray properties of a sample of 19 high redshift ($1 < z < 2$) FRI candidates selected on the basis of the radio flux (Chiaberge et al. 2009) and observed in the Chandra COSMOS field. From the spectroscopic and photometric redshift found in the literature, we find that the rest frame 1.4GHz radio luminosities of our 19 FRI candidates span a range from $\sim 2 L_{break}(1.4GHz)$ down to $\sim 0.05 L_{break}$.

We find that 6 of our radio sources have an unresolved

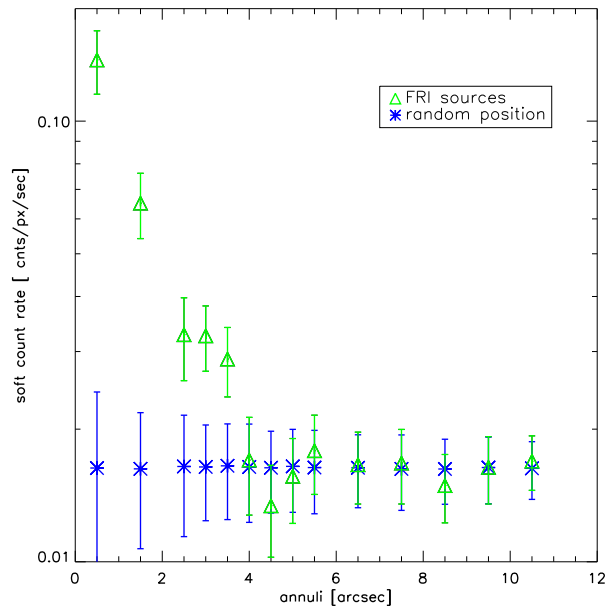


Figure 4. Radial profile in the soft band of the stacked image of the 19 FRI sources (green triangles) compared with the radial profile measured in random fields (blue asterisks).

X-ray counterpart in the C-COSMOS catalog. Two additional radio sources have a significant X-ray detection in our aperture photometry, even though they are not included in the C-COSMOS catalog. We also search for unresolved X-ray emission below the detection threshold by stacking the X-ray images in the position of the 11 FRI radio sources without X-ray counterparts. We find a 2σ detection in the soft band, and none in the hard band.

We performed the X-ray spectral analysis of the FRI galaxies with X-ray counterpart. We find that source FRI 3, which has the highest S/N, has a significant intrinsic absorption $N_H = (3.5 \pm 0.5) \times 10^{23} \text{ cm}^{-2}$. The tentative spectral analysis of the other X-ray sources suggest intrinsic absorption in the range $10^{22} - 10^{23} \text{ cm}^{-2}$, as suggested also by the HR of their stacked signal. However, we can not infer that FRI galaxies at high redshift preferentially have X-ray absorbed spectra, since such a conclusion should be based on a complete FRI sample and on deeper X-ray data.

The X-ray luminosities of the FRI candidates show values that, although occasionally observed in low redshift FRIs (Donato et al. 2004, Balmaverde et al. 2008), appear to be higher than the typical FRI X-ray luminosities in the local universe. This finding should be regarded as tentative since it is based on a sample with 11 X-ray upper limits out of 19 sources. Nevertheless, our study suggests an evolution of the X-ray properties of FRI sources with redshift, with accretion at high redshift possibly being more efficient than in low redshift ones.

We also search for extended X-ray emission possibly associated to the ICM of the virialized haloes hosting the FRIs. We compute radial profiles in several bins around the FRI positions, and find that the stacked image is consistent with unresolved emission, with no signs of diffuse X-ray signal. To put an upper limit to the ICM emission around FRIs, we compute mock images assuming the presence of a virialized

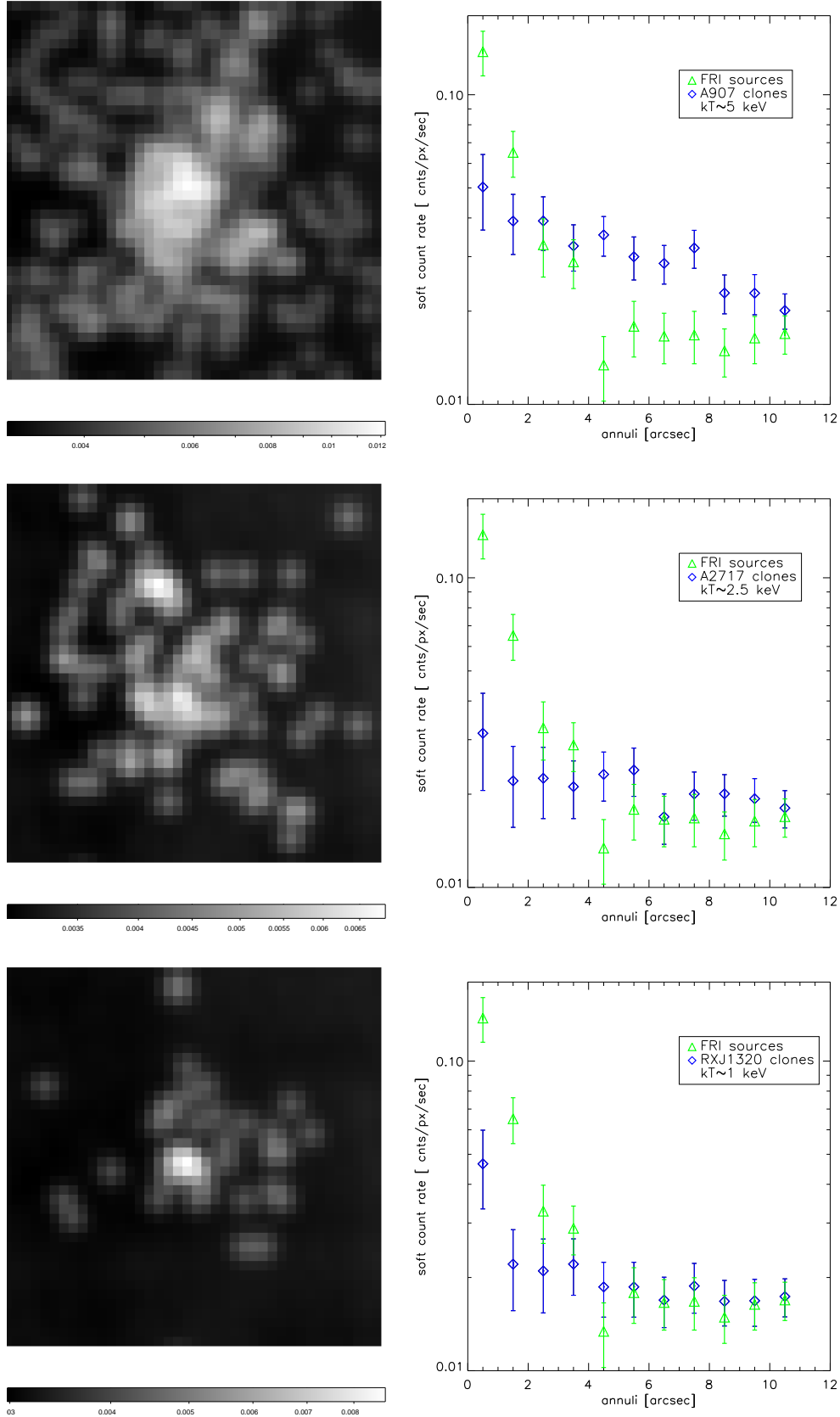


Figure 5. Upper left panel: soft-band, smoothed stacked image assuming virialized haloes with $kT \simeq 5$ keV in the position of the FRI sources; upper right panel: count rate radial profile for the mock image (blue diamonds) compared with the radial profile found in the stacked image of the FRI sources (green triangles). Middle panels: the same as the upper panels assuming virialized haloes with $kT \simeq 2.5$ keV. Bottom panels: the same as the upper panels assuming virialized haloes with $kT \simeq 1$ keV. The size of the images is 40×40 arcsec.

halo of 5, 2.5 and 1 keV at the position of each FRI. The mock images are obtained by stacking the images of real Chandra clusters, each cloned at the redshift and with an exposure matching those of the corresponding source. We exclude the presence of high temperature virialized haloes with $kT \simeq 5$ keV. On the other hand, there is still room for ICM emission from medium and low temperature ICM (1 – 2.5 keV).

The results of this study show that the X-ray analysis of FRI sources at high redshift can shed light on several aspects, in particular the physics of accretion processes in FRIs and the presence of virialized haloes hosting the FRI galaxies. However, in order to confirm the hint of higher intrinsic absorption and higher luminosities in high- z FRIs, and further explore the presence of ICM around them, we need deeper X-ray data and larger FRI sample. Considering the stacked signal of the non X-ray detected sources, an exposure of 1 Msec with Chandra would guarantee at least the detection (~ 10 net counts) of the majority of the sample and a robust X-ray spectral analysis (≥ 100 net counts) for at least 1/3 of the sample. The best field where this study can be extended is the Chandra Deep Field South with 4Ms of Chandra time, which has, however, a ten times smaller solid angle. This study is currently underway.

ACKNOWLEDGMENTS

We acknowledge support from ASI-INAF I/088/06/0 and ASI-INAF I/009/10/0. PT acknowledges support under the grant INFN PD51. We thank Joana Santos for providing the high- z clones of local X-ray clusters observed with Chandra. We thank Gianluca Castignani for the providing the radio luminosity of the FRI sample, and Piero Rosati for helpful discussions. We also thank Francesca Civano e Giorgio Lanzuisi for discussion on the spectral analysis of C-COSMOS sources. Finally, we thank the anonymous referee for detailed and helpful comments.

REFERENCES

- Andreon S., Huertas-Company M., 2011, *A&A*, 526, A11
 Antonucci R., 1993, *ARA&A*, 31, 473
 Balmaverde B., Baldi R. D., Capetti A., 2008, *A&A*, 486, 119
 Balmaverde B., Capetti A., Grandi P., 2006, *A&A*, 451, 35
 Barkhouse W. A., et al., 2006, *ApJ*, 645, 955
 Becker R. H., White R. L., Helfand D. J., 1995, *ApJ*, 450, 559
 Best P. N., von der Linden A., Kauffmann G., Heckman T. M., Kaiser C. R., 2007, *MNRAS*, 379, 894
 Blackburn J. K., 1995, *ASPC*, 77, 367
 Blandford R. D., Payne D. G., 1982, *MNRAS*, 199, 883
 Capetti A., Fanti R., Parma P., 1995, *A&A*, 300, 643
 Cappelluti N., et al., 2009, *A&A*, 497, 635
 Cash W., 1979, *ApJ*, 228, 939
 Chiaberge M., Capetti A., Celotti A., 1999, *A&A*, 349, 77
 Chiaberge M., Capetti A., Macchetto F. D., Rosati P., Tozzi P., Tremblay G. R., 2010, *ApJ*, 710, L107
 Chiaberge M., Tremblay G., Capetti A., Macchetto F. D., Tozzi P., Sparks W. B., 2009, *ApJ*, 696, 1103
 Demarco R., et al., 2010, *ApJ*, 711, 1185
 Donato D., Sambruna R. M., Gliozzi M., 2004, *ApJ*, 617, 915
 Donzelli C. J., Chiaberge M., Macchetto F. D., Madrid J. P., Capetti A., Marchesini D., 2007, *ApJ*, 667, 780
 Eisenhardt P. R. M., et al., 2008, *ApJ*, 684, 905
 Elvis M., et al., 2009, *ApJS*, 184, 158
 Evans D. A., Hardcastle M. J., Croston J. H., 2008, *ASPC*, 386, 161
 Evans D. A., Worrall D. M., Hardcastle M. J., Kraft R. P., Birkinshaw M., 2006, *ApJ*, 642, 96
 Fabian A. C., Celotti A., Erlund M. C., 2006, *MNRAS*, 373, L16
 Fanaroff B. L., Riley J. M., 1974, *MNRAS*, 167, 31P
 Ferrarese L., Merritt D., 2000, *ApJ*, 539, L9
 Gawroński M. P., Marecki A., Kunert-Bajraszewska M., Kus A. J., 2006, *A&A*, 447, 63
 Gebhardt K., et al., 2000, *ApJ*, 539, L13
 Gehrels N., 1986, *ApJ*, 303, 336
 Ghisellini G., Celotti A., 2001, *A&A*, 379, L1
 Gladders M. D., Yee H. K. C., 2000, *AJ*, 120, 2148
 Gopal-Krishna, Wiita P. J., 2000, *A&A*, 363, 507
 Hardcastle M. J., Worrall D. M., Birkinshaw M., Laing R. A., Bridle A. H., 2002, *MNRAS*, 334, 182
 Hasinger G., et al., 2007, *ApJS*, 172, 29
 Hill G. J., Lilly S. J., 1991, *ApJ*, 367, 1
 Hopkins P. F., Somerville R. S., Hernquist L., Cox T. J., Robertson B., Li Y., 2006, *ApJ*, 652, 864
 Ilbert O., et al., 2009, *ApJ*, 690, 1236
 Jackson C. A., Wall J. V., 1999, *MNRAS*, 304, 160
 Kaiser C. R., Alexander P., 1997, *MNRAS*, 286, 215
 Kalberla P. M. W., Burton W. B., Hartmann D., Arnal E. M., Bajaja E., Morras R., Pöppel W. G. L., 2005, *A&A*, 440, 775
 Komatsu E., et al., 2011, *ApJS*, 192, 18
 Ledlow M. J., Owen F. N., 1996, *AJ*, 112, 9
 Lilly S. J., et al., 2007, *ApJS*, 172, 70
 Livio M., 1999, *PhR*, 311, 225
 Muzzin A., et al., 2009, *ApJ*, 698, 1934
 Nousek J. A., Shue D. R., 1989, *ApJ*, 342, 1207
 Owen F. N., 1996, *IAUS*, 175, 305
 Owen F. N., Ledlow M. J., 1994, *ASPC*, 54, 319
 Pierre M., Valtchanov I., Refregier A., 2002, *astro*, arXiv:astro-ph/0202117
 Prestage R. M., Peacock J. A., 1988, *MNRAS*, 230, 131
 Reynolds C. S., Fabian A. C., Celotti A., Rees M. J., 1996, *MNRAS*, 283, 873
 Rosati P., Borgani S., Norman C., 2002, *ARA&A*, 40, 539
 Salvato M., et al., 2011, *arXiv*, arXiv:1108.6061
 Santos J. S., Rosati P., Tozzi P., Böhringer H., Ettori S., Bignamini A., 2008, *A&A*, 483, 35
 Scarpa R., Urry C. M., 2001, *ApJ*, 556, 749
 Schinnerer E., et al., 2007, *ApJS*, 172, 46
 Scoville N., et al., 2007, *ApJS*, 172, 150
 Tanaka M., Finoguenov A., Ueda Y., 2010, *ApJ*, 716, L152
 Tozzi P., et al., 2006, *A&A*, 451, 457
 Tozzi P., et al., 2001, *ApJ*, 562, 42
 Tremaine S., et al., 2002, *ApJ*, 574, 740
 Trump J. R., et al., 2007, *ApJS*, 172, 383
 Urry C. M., Padovani P., 1995, *PASP*, 107, 803
 Wilson G., et al., 2009, *ApJ*, 698, 1943
 Xue Y. Q., et al., 2011, *ApJS*, 195, 10
 Zirbel E. L., 1996, *ApJ*, 473, 713

This paper has been typeset from a \TeX / \LaTeX file prepared by the author.